

www.acsaem.org Article

Enhanced Lithium Storage of an Organic Cathode via the Bipolar Mechanism

Tianyuan Liu,[#] Ki Chul Kim,[#] Byeongyong Lee,[#] Shikai Jin, Michael J. Lee, Mochen Li, Suguru Noda, Seung Soon Jang,^{*} and Seung Woo Lee^{*}



Cite This: ACS Appl. Energy Mater. 2020, 3, 3728-3735



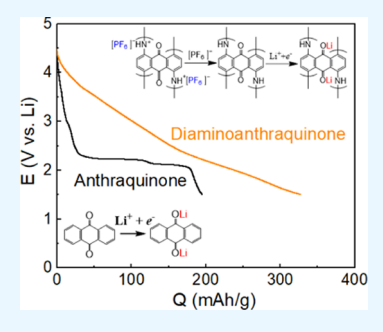
ACCESS

Metrics & More

Article Recommendations

s Supporting Information

ABSTRACT: Electrochemically polymerized anthraquinone derivatives on conductive carbon nanotubes are redox-active as organic cathode materials for lithium-ion batteries. Density functional theory calculations and electrochemical measurements reveal that the polymerized anthraquinone cathodes exhibit the multiple redox reactions with electrolyte ions through a bipolar charge storage mechanism: (1) the n-type doping/dedoping mechanism associated with Li⁺ binding in a potential window of 1.5–3.0 V versus Li and (2) the PF₆⁻-involved p-type doping/dedoping mechanism in a potential window of 3.0–4.5 V versus Li. Polymerized 1-aminoanthraquinone (AAQ) shows progressive deactivation upon cycling because of the charge trapping effect. On the other hand, the polymerized 1,5-diaminoanthraquinone (DAAQ) delivers extraordinarily high charge capacities up to 311 mA h/g while effectively avoiding undesirable charge trapping behaviors. We establish the relationship between the structure and



charge storage performance of the polymerized quinone derivatives, suggesting a high-performance organic cathode material for rechargeable battery applications.

KEYWORDS: Li-ion batteries, cathodes, organic electrode materials, charge storage mechanism, charge trapping effect

■ INTRODUCTION

High-performance rechargeable batteries are essential to support the rapidly growing large-scale electrochemical energy storage applications such as electric vehicles and grid-scale energy storage systems. Considering the cost and performance, lithium-ion batteries (LIBs) are a state-of-the-art technology that uses lithium transition metal oxides or metal phosphates for the cathode materials and graphite for the anode material.² However, inorganic-based cathode materials rely on high-cost cobalt and require a high carbon footprint for their production,³ driving the use of more cost-effective and sustainable electrode materials. Recently, organic electrode materials have received considerable attention for replacing inorganic-based cathode materials with earth-abundant materials with high capacity and low-toxicity. 4-6 In particular, carbonyl-based compounds are considered the most promising organic electrode because of the highly reversible redox active nature. 5,7,8 Therefore, tremendous efforts have been devoted to develop carbonyl-based organic cathodes, which have accomplished high specific capacities up to 580 mA h/g. 5,9-11 However, the high solubility of small organic molecules in organic electrolytes is a major drawback to be resolved for the use in rechargeable batteries.

Polymerization that incorporates redox-active structures into an insoluble but swellable polymeric environment is regarded as a promising strategy to prevent the molecular dissolution. ^{8,12} Therefore, various carbonyl-based polymeric environments, such as nitrogen-containing polycyclic quinones, ¹³ polymerized

dihydroxy-benzoquinonyl sulfides,¹⁴ aromatic carbonyl sulfide polymers,¹⁵ and anthraquinone derivatives,^{16–21} have been suggested as insoluble organic cathodes. However, charges could be irreversibly trapped in certain redox-active polymers, which is called the charge-trapping effect, inducing a gradual loss of capacity during cycling.^{22–25} For example, a recent study on p/n-dopable conducting polymers containing anthraquinone moieties showed that the cation charge trapping on quinone groups during the n-doping process is a major cause of performance degradation for the supercapacitor applications.²⁶ Therefore, in order to overcome such an undesirable behavior, it is crucial to understand the relationship between the chemical structure of polymerized carbonyl electrodes and their charge storage properties.

In this study, anthraquinone derivatives are mixed with conductive carbon nanotubes and electrochemically polymerized to study the energy storage mechanism and performance, particularly, to assess their potential as cathode for LIBs. Electrochemical characterizations and density functional theory (DFT) calculations reveal that amine functional groups in monomeric units of 1-aminoanthraquinone (AAQ) and 1,5-

Received: January 28, 2020 Accepted: April 1, 2020 Published: April 1, 2020





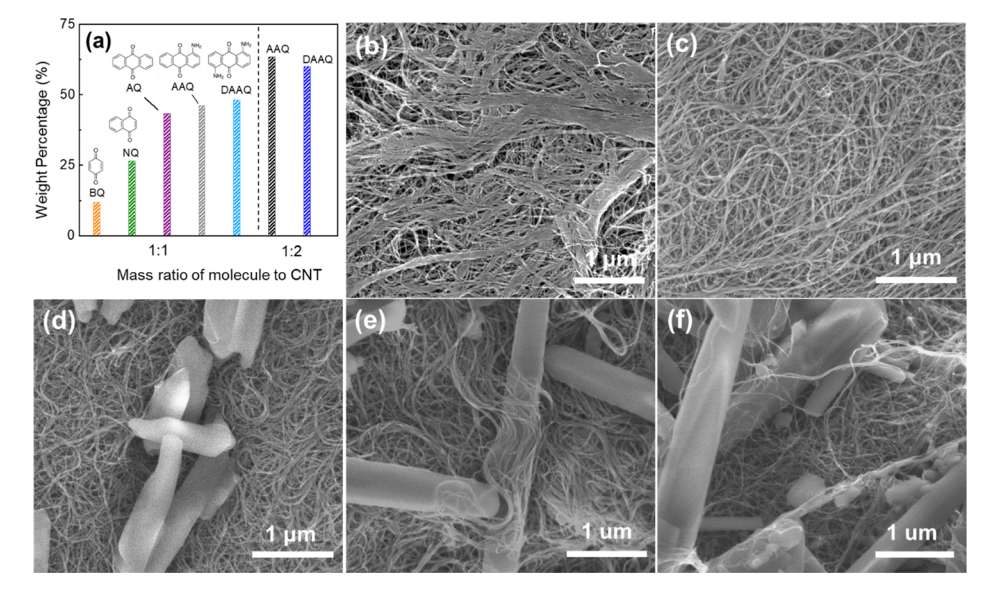


Figure 1. (a) Weight percentages of molecules in various composite films. SEM images of (b) pristine FWNT films and (c-f) various composite films. Composite films consist of (c) FWNTs and anthraquinone (AQ-NT), (d) FWNTs and 1-aminoanthraquinone (AAQ-NT), (e,f) FWNTs and 1,5-diaminoanthraquinone (DAAQ-NT). These films were obtained through vacuum filtration of aqueous dispersions of FWNTs or aqueous mixtures of FWNTs and various molecules. The mass ratio between molecules and FWNTs were 1:1 in (c-e), and 2:1 in (f).

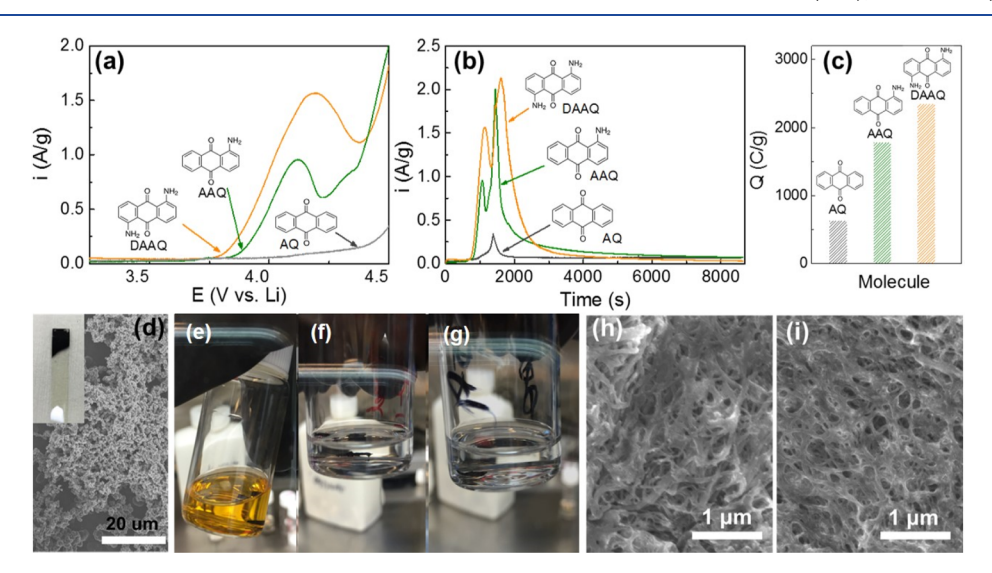


Figure 2. (a) LSV of various composite films containing different molecules, namely AQ, AAQ, and DAAQ from open circuit voltage to 4.5 V vs Li at a scan rate of 1 mV/s. (b) Anodic current as a function of time for the composite films. (c) Charges (normalized by the mass of organic molecules) transferred during the LSV and potentiostatic polymerization process for different composite films. (d) SEM image of the polymeric films formed on ITO after 10 mM DAAQ was potentiostatically polymerized in a three-electrode cell using Li foils as both counter and reference electrodes. Inset is the digital image of the black polymer films. (e) Digital image showing the change in the color of the solution containing a colorless blank electrolyte (EC/DMC mixture, 3/7, v/v) driven by a piece of the DAAQ-NT film dipped into the solution. Digital images showing the electrochemical polymerization of DAAQ-NT films with DAAQ loadings of (f) 48 and (g) 60 wt % in mixtures of EC/DMC (3:7, v/v) for 1 h. SEM images of polymerized poly-DAAQ-NT films with DAAQ loadings of (h) 48 and (i) 60 wt %.

diaminoanthraquinone (DAAQ) polymers play a critical role in generating secondary amines for the bipolar charge storage mechanism with both electrolyte cation (Li⁺) and anions (PF₆⁻). We further emphasize that the charge trapping phenomena, which are distinctly observed from AAQ polymers, would be associated with the kinetic limitation in the diffusion of strongly adsorbed Li as well as the high electronic charge transfer resistance. The polymerized DAAQ-based hybrid films exhibit a high capacity of \sim 311 mA h/g with superior rate capability by effectively utilizing the bipolar charge storage mechanism, thereby proposing a high-performance cathode for rechargeable battery applications.

RESULT AND DISCUSSION

Five quinone derivatives such as p-benzoquinone (BQ), 1,4-naphthoquinone (NQ), anthraquinone (AQ), AAQ, and DAAQ were individually mixed with few-walled carbon nanotubes (FWNTs) 27,28 in water, and the aqueous mixtures were vacuum filtered to fabricate free-standing hybrid films. During the solution process, the quinone derivatives can be attached to the surface of FWNTs by the π - π interactions. When organic molecules and FWNTs were initially mixed into the solution at 1:1 mass ratio, the weight percent of organic molecules remaining in the hybrid film increased with the size

of the molecule: 11.7 wt % for BQ, 26.5 wt % for NQ, 43.3 wt % for AQ, 46 wt % for AAQ, and 48 wt % for DAAQ, respectively (Figure 1a). This trend can be explained by the stronger $\pi - \pi$ interaction between larger quinone derivative and FWNTs. Additionally, when the mass ratio between the organic molecule and FWNT increased from 1:1 to 2:1, the weight percentages of adsorbed AAQ and DAAQ on FWNTs further increased to 63.4 and 60 wt %, respectively. The scanning electron microscopy (SEM) image shows that the pristine FWNT film attains a randomly packed network structure where large FWNT bundles are easily observed because of the poor dispersion of FWNTs in water (Figure 1b). However, when AQ was incorporated in the hybrid film, the large bundles disappeared. Such a change in the morphology may be due to the adhesion of AQ molecules on the surface of FWNT, which can disrupt the $\pi-\pi$ interaction between the FWNTs (Figure 1c). Interestingly, rod-like supramolecular assemblies were also observed in the hybrid films containing AAQ (Figures 1d and S1a,b) and DAAQ (Figures 1e,f and S1c,d). More rods were observed in the hybrid films with higher AAQ (63.4 wt %) and DAAQ (60 wt %) loadings (Figure S1b,d). The formation of these rods also may be attributed to the combination of intermolecular hydrogen bonding²⁹ and $\pi - \pi$ interactions between quinone derivatives (Figure S2).

The electrochemical polymerization behavior of anthraquinone derivatives in the hybrid films was investigated by linear sweep voltammetry (LSV) from an open circuit potential (~3.2 V vs Li) to 4.5 V versus Li in a two-electrode cell using a Li foil as a counter electrode (Figures 2a and S3a). AQ showed a small anodic current, while both AAQ and DAAQ exhibited a strong anodic polymerization current (Figures 2a and S3a). The electrochemical polymerization process of AAQ and DAAQ is similar to that of aniline through the anodic oxidation process.30 The previous study on DAAQ also suggested that the electrochemical polymerization of DAAQ occurred primarily at 1,4 and 5,8 positions, which is similar to that of polyaniline with a head-to-tail structure.³¹ To completely polymerize the available molecules in the hybrid films, a potentiostatic polymerization process was followed by holding the potential at 4.5 V versus Li for 2 h (Figures 2b and S3b,c). Similar to the trend from LSV, both AAQ and DAAQ showed much higher anodic current than AQ during the potentiostatic polymerization process. The total amount of charge passed per unit mass of the molecule during the polymerization process showed a strong correlation with the number of amino groups on the molecule (Figures 2c and S3d) indicating the critical role of amino groups in the polymerization process. In addition, the electrochemical polymerization of DAAQ was further demonstrated on an indium tin oxide (ITO) substrate with a three-electrode Swagelok-type cell using Li foils as both counter and reference electrodes. After a potential holding process at 4.5 V versus Li, a polymeric film was deposited on the ITO substrate (Figure 2d). The polymerized DAAQ was investigated by X-ray photoelectron spectroscopy and Fourier transform infrared (FTIR) spectroscopy measurements (Figure S4). The N 1s spectrum for polymerized DAAQ was fitted by peaks of quinonoid imine (=N-, 398.5 eV), benzenoid amine (-NH-, 399.5 eV), and protonated N⁺ (400.7 eV).³² The FTIR spectra showed two sharp peaks at 3419 and 3309 cm⁻¹ associated with -NH₂ groups, but these peaks disappeared after the polymerization,

indicating that polymerized DAAQ has a similar backbone structure to polyaniline (Figure S4b). 30

The solubility tests of DAAQ in the hybrid films were performed before and after the polymerization process following the previous study.³³ When a piece of the hybrid film consisting of adsorbed DAAQ and FWNT (DAAQ-NT) was immersed in a colorless organic solvent, a mixture of ethylene carbonate (EC) and dimethyl carbonate (DMC) (3/ 7, v/v), the color of the solvent immediately turned into a light yellow because of the dissolution of DAAQ, resulting in the loss of active materials (Figure 2e). On the contrary, no color change was observed for the polymerized DAAQ on FWNT (poly-DAAQ-NT) with different loadings (48 and 60 wt %) for 1 h, indicating that the dissolution issue of active molecules can be successfully depressed by the in situ electrochemical polymerization process (Figure 2f,g). After the electrochemical polymerization, the rod-like assemblies of molecules disappeared, and a smooth polymer film was formed within the FWNT networks (Figure 2h,i). In this nano-architecture, porous and conductive FWNTs can provide fast ion and electron transport for the redox reaction of polymerized DAAQ. We also conducted the potentiodynamic polymerization of DAAQ-NT films in the potential range of 4.0-4.5 V versus Li and a scan rate of 5 mV/s for 36 cycles. During the potentiodynamic polymerization process, the anodic current gradually decreased toward the steady state (Figure S5), visualizing the gradual anodic polymerization process during the cyclic voltammetry (CV) cycles. Comparing with the potentiostatic polymerization procedure, the potentiodynamic polymerization achieved significantly better capacity retention for samples with 48 and 60 wt % DAAQ loadings after 10 cycles (Figure 4d). This indicates that a more optimized polymer structure can be formed through the potentiodynamic process for reversible charge storage.

The DFT method was employed to study the redox potentials for the monomers of the two quinones (AAQ and DAAQ) and their dimers to elucidate the redox properties of the electrochemically polymerized quinones in the hybrid films (Figure 3). The detailed information on the calculated redox potentials and electronic properties can be found in Tables S1 and S2 in the Supporting Information. In the fully charged state (i.e., molecules without Li binding), both quinones showed a redox potential of 2.0-2.2 V versus Li, with a slight decrease in the number of amine groups. The redox potentials gradually decreased as the number of bound Li ions increased during the discharging process, becoming negative or close to zero after binding with two and four Li ions for monomeric and dimeric units, respectively. These results evidently indicate that they lose the cathodic character. From a structural point of view, the monomers and dimers can store two and four Li ions near the redox-active carbonyls, respectively. In particular, it is noted that each dimer has the most thermodynamically favorable site in the center of the molecule consisting of two electron-rich carbonyls, which can accommodate multiple Li ions near the center of the molecule. Considering the presence of the secondary amine moiety in the backbone of AAQ and DAAQ polymers, the electrolyte anion (PF₆⁻)-involved p-type charge storage mechanism in polyaniline is also expected from the AAQ and DAAQ polymers. Our further DFT computation shows that the p-type doping/dedoping process occurs at 3.9 V versus Li for the AAQ dimer with one bound PF₆ anion and 3.8 and 4.5 V versus Li for the DAAQ dimer with one and two bound PF₆⁻ anion(s), respectively (Figure 3). These computa-

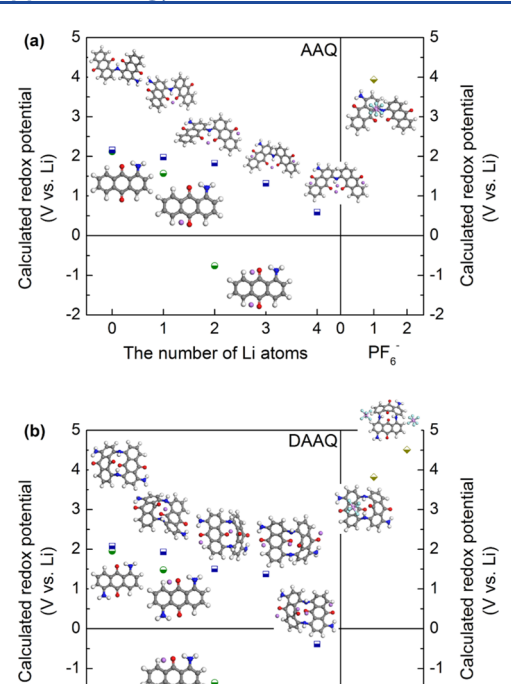


Figure 3. Calculated redox potentials for monomers and dimers of (a) AAQ and (b) DAAQ as a function of the number of bonded electrolyte ions (i.e., Li and PF₆ ions). Note that the p-type doping/dedoping mechanism is related to the interaction between PF₆ anions and secondary amines in dimers.

3

The number of Li atoms

0

2

PF

tional results highlight the multiple redox reactions of the AAQ and DAAQ polymers with electrolyte ions (i.e., Li and PF₆ ions) in the broad potential range of 2.0–4.5 V versus Li. The different redox behaviors of the aforementioned organic complexes can be further understood through strong linear correlations of the calculated redox potential with an electron affinity and the lowest occupied molecular orbital energy, which is consistent with previous computational studies (Figure S6). $^{7,8,34-38}$

The electrochemical properties of AQ, polymerized AAQ and DAAQ were investigated by CV measurements (Figures 4a-c, S7 and S12). The first CV scans of both AAQ and DAAQ polymers showed clear redox peaks in the potential range of 1.7-2.5 V versus Li that are ascribed to the multiple redox reactions between carbonyl groups and Li ions, showing good agreement with the DFT computation results. In addition, p-type doping/dedoping peaks associated with the redox reactions between secondary amines and PF₆⁻ anions were also observed in the high potential region of 3.6-3.8 V versus Li as predicted by the DFT computations. Additionally, the AAQ polymer showed a much larger reduction peak compared to the small oxidation peak (Figure 4a). Upon subsequent CV cycling, these redox peaks gradually decreased and eventually showed negligible redox peaks in the low potential region of 1.5-2.5 V versus Li. The asymmetric redox peaks from the AAQ indicate the charge (Li⁺-e⁻ pairs) trapping effect in the polymer during the discharge process due to the strong binding environment. Therefore, carbonyl groups in the polymerized AAQ were gradually occupied by the trapped charge carriers, and finally, the most redox-active sites are occupied in the reduced state after CV cycles. On the other hand, the polymerized DAAQ by both potentiostatic and

potentiodynamic methods showed much symmetric redox behaviors than AAQ, and maintained a stable redox peak around 2 V versus Li upon the continuous cycles (Figure 4b,c). After 10 cycles, the poly-DAAQ-NT exhibited a significantly higher capacitance of 287 F/g compared to that of the polymerized AAQ (74 F/g) (Figures 4d and S8), indicating that the mitigation of the charge trapping is very important to improve the performance of carbonyl-based polymer electrodes. Before the CV cycle, AAQ and DAAQ polymers showed very similar Nyquist plots (Figure 4e,f). For both AAQ and DAAQ, the reduced charge transfer resistance after cycling compared to their initial state may be attributed to the anion doping effect observed in the conducting polymers.³⁹ However, the DAAQ polymer exhibited a much smaller charge transfer resistance (R_{ct} , 190 Ω) than AAQ polymer (R_{ct} , 954 Ω). This suggests that the charge trapping behavior in the polymerized AAQ increases the charge transfer resistance and leads to the loss in the redox activity of the carbonyl groups.

To better understand the charge trapping behaviors in carbonyl polymers, the DFT modeling approach was employed to calculate the binding strength and diffusivity of Li at the molecular level. Two structural models were prepared to describe the AAQ and DAAQ dimers with one Li bound to the most thermodynamically favorable binding site that is surrounded by two central carbonyls. Next, to understand the difference in the recharging process between the two polymers, we calculated the Li binding free energies in vacuum and electrolyte solution (thermodynamic parameter, Figure 4g) and the activation energy barriers (kinetic parameter, Figure 4h) associated with the Li diffusion process escaping from the binding site. Figure 4h shows the potential energy surface during the Li diffusion process, while Figure 4i shows the structural change of the dimers induced by the Li diffusion process. Figure S9 in the Supporting Information shows the stepwise structural changes of AAQ and DAAQ during the Lidiffusive recharging process, more in detail. Thermodynamically, the AAQ dimer has a stronger Li binding free energy with Li (-84.8 kcal/mol) in the electrolyte solution than the DAAQ dimer (-53.8 kcal/mol). Kinetically, the activation energy barrier (191.31 kJ/mol) for the Li escaping from the AAQ dimer is much higher than that from the DAAQ dimer (158.98 kJ/mol). More importantly, the relatively high activation energy barrier for AAQ as compared with DAAQ can be further rationalized by the structural Li trapping behavior in AAQ. During the Li diffusion process, the highly flexible AAQ dimer, in which two monomers are linked by one secondary amine moiety, can undergo significant structural changes (i.e., independent rotation of each monomer) to hold a bound Li. In contrast, the DAAQ dimer has limited structural mobility during the Li diffusion process because of the conformational invariability of two monomeric units through two secondary amine linkers. All these results highlight the difference in the charge trapping behavior between AAQ and DAAQ in terms of thermodynamic, kinetic, and structural perspectives.

The bipolar charge storage mechanism of polymerized DAAQ can be clearly visualized by potential-dependent CV measurements (Figure 5a). In the low potential region of 1.5—3 V versus Li, the CV scan displayed a clear redox peak around 2 V versus Li that is ascribed to the reversible redox reaction between the quinone groups and Li ions. On the other hand, in the high potential region of 3–4.5 V versus Li, the p-type doping/dedoping mechanism involving the interaction be-

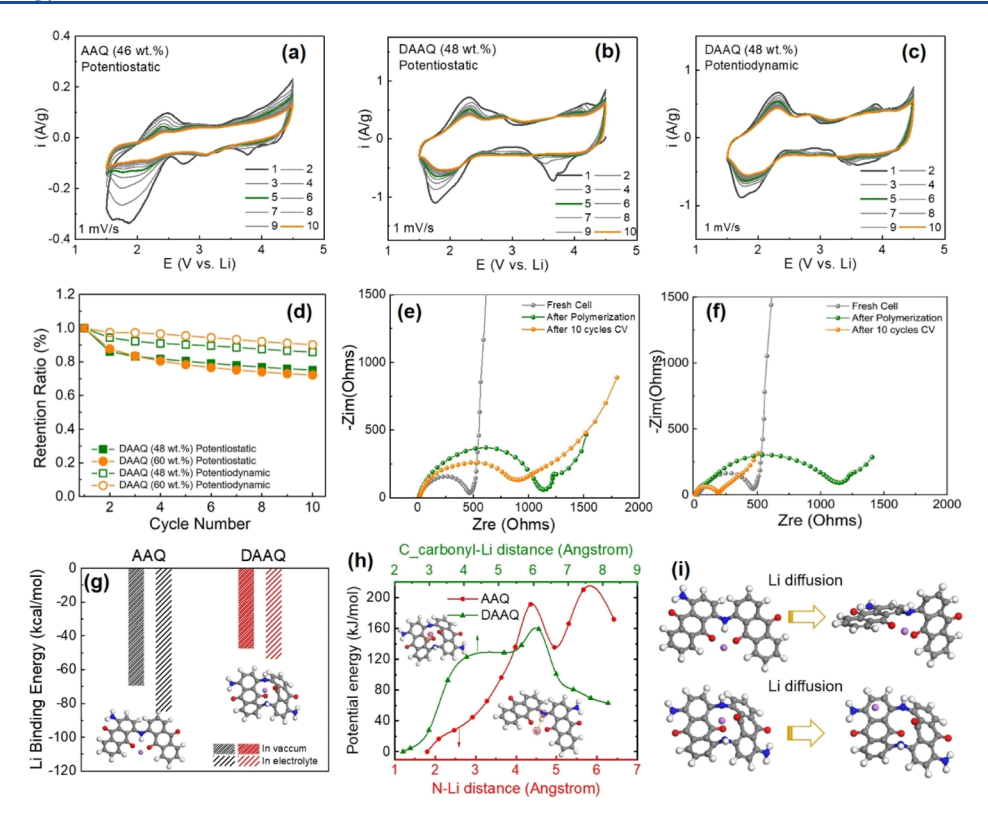


Figure 4. Cyclic voltammetry scans for hybrid films containing potentiostatically-polymerized (a) AAQ, (b) DAAQ (48 wt %), and (c) DAAQ (60 wt %). (d) Capacitance retention of the poly-DAAQ-NT films with DAAQ loadings of 48 and 60 wt % after being either potentiodynamically or potentiostatically polymerized. Nyquist plots drawn by electrochemical impedance spectroscopy for the polymerized (e) poly-AAQ-NT and (f) poly-DAAQ-NT films. (g) Computed binding free energies in vacuum and the electrolyte solution of Li to the AAQ and DAAQ dimers. (h) Potential energy surfaces associated with the diffusion processes of Li escaping from the most redox-active binding sites for the AAQ and DAAQ dimers. (i) Structural geometries before and after Li escapes from the AAQ and DAAQ dimers.

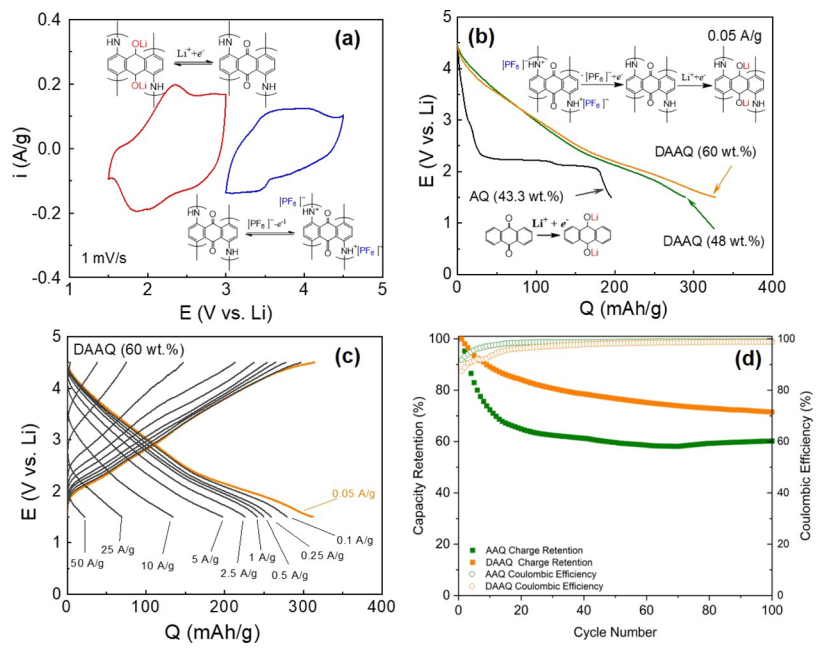


Figure 5. (a) Potential-dependent CV scans of the polymerized poly-DAAQ-NT films at a scan rate of 1 mV/s. (b) Comparison of the discharge profiles of the AQ-NT and polymerized poly-DAAQ-NT films. (c) Rate-dependent galvanostatic charge and discharge profiles of the poly-DAAQ-NT films with DAAQ loadings of 60 wt %. The electrode was potentiodynamically polymerized for 36 cycles between 4.0 and 4.5 V vs Li at a scan rate of 5 mV/s. (d) Capacity retention of the AAQ and DAAQ hybrid film (60 wt %) at 1 A/g for 100 cycles.

tween secondary amines and the PF₆⁻ anion was observed. We further evaluated the charge storage performance of the

potentiodynamically polymerized poly-DAAQ-NT film using galvanostatic charge/discharge tests. The specific capacity of

the hybrid film significantly increased from 195 mAh/g for the AQ-NT film to 291 and 311 mA h/g for the poly-DAAQ-NT films with polymer loadings of 48 and 60 wt % at a current rate of 0.05 A/g, respectively (Figures 5b and S10). The capacity contribution of the FWCNT was studied separately and corresponded to a small fraction of ~18.3% of the total capacity for the poly-DAAQ-NT film (60 wt %) at 0.05A/g (Figure S11). We postulate that the sloped discharge profiles for the poly-DAAQ-NT films are due to various local environments of the redox-active sites, including varied polymer chain lengths and configurations, whereas the prominent potential plateau in the discharge profile for the AQ-NT arises from the consistent environment and structure of the monomers for the redox reaction. The rate-capabilities of poly-DAAQ-NT films were further evaluated at various current densities from 0.05 to 50 A/g (Figures 5c and S10). The poly-DAAQ-NT films maintained their high capacities of 232-241 mA h/g at 1 A/g and 125-134 mA h/g at even 10 A/g, demonstrating a superior rate-performance. Such high capacity and excellent rate-capability of the poly-DAAQ-NT film significantly outperformed the performance of previously reported quinone-based polymer electrodes (Table S3). In addition, the Coulombic efficiency was calculated to be 99.4% at 1 A/g and 95% at 10 A/g with the round-trip energy efficiency of 77-79% for the poly-DAAQ-NT film. Finally, the capacity of the poly-DAAQ-NT and poly-AAQ-NT films were compared at a high current rate of 1 A/g for 100 cycles to evaluate the cycling stability (Figure 5d). The poly-DAAQ-NT film exhibited a capacity retention of 72%, which was higher than that of the poly-AAQ-NT film (60%). Such improved cycling stability of polymerized DAAQ compared to polymerized AAQ can be attributed to much less charge trapping effect. The extended cycling test was also performed for poly-DAAQ-NT at 1 A/g up to 500 cycles (Figure S13), and the hybrid film still maintained a high discharge capacity of \sim 184.5 mA h/g with a Coulombic efficiency of 99.1%.

CONCLUSIONS

In summary, we have demonstrated that the polymeric forms of (di)amino-anthraquinones can be utilized as high-performance organic cathode materials through the bipolar mechanism for LIBs. Redox properties and battery performances of AAQ and DAAQ polymers were correlated with their structures using both experimental and DFT modeling approaches. We showed that the AAQ polymer suffered from poor cycling stability because of the charge trapping behaviors, while the DAAQ polymer could exhibit a high capacity up to 311 mA h/g with superior rate capability by effectively utilizing the bipolar mechanism. The results highlight the importance of the molecular design of the redox-active polymer to enhance the charge storage performance for rechargeable battery applications.

ASSOCIATED CONTENT

Supporting Information

The Supporting Information is available free of charge at https://pubs.acs.org/doi/10.1021/acsaem.0c00187.

Calculated redox potentials for AAQ and DAAQ monomers with/without bound Li atom(s) and their electronic properties; calculated redox potentials for AAQ and DAAQ dimers with/without bound electrolyte ion(s); SEM images of composite films; schematic

illustrations of feasible hydrogen bonding networks; LSV measurements; high-resolution XPS spectra and FTIR spectroscopy; CV scans of the potentiodynamic polymerization process; calculated redox potentials of AAQ and DAAQ monomers; CV scans for hybrid films; CV measurement; potential energy surfaces for Li diffusion; rate-dependent galvanostatic charge and discharge profiles; CV scans for the AQ-NT film; and comparison of electrochemical performances of various organic electrodes (PDF)

AUTHOR INFORMATION

Corresponding Authors

Seung Soon Jang — Computational NanoBio Technology Laboratory, School of Materials Science and Engineering, Georgia Institute of Technology, Atlanta, Georgia 30332, United States; Occid.org/0000-0002-1920-421X; Email: seungsoon.jang@mse.gatech.edu

Seung Woo Lee − G. W. Woodruff School of Mechanical Engineering, Georgia Institute of Technology, Atlanta, Georgia 30332, United States; orcid.org/0000-0002-2695-7105; Email: seung.lee@me.gatech.edu

Authors

Tianyuan Liu – G. W. Woodruff School of Mechanical Engineering, Georgia Institute of Technology, Atlanta, Georgia 30332, United States

Ki Chul Kim – Division of Chemical Engineering, Konkuk University, Seoul 05029, The Republic of Korea

Byeongyong Lee − G. W. Woodruff School of Mechanical Engineering, Georgia Institute of Technology, Atlanta, Georgia 30332, United States; School of Mechanical Engineering, Pusan National University, Busan 46241, The Republic of Korea; orcid.org/0000-0002-3548-3642

Shikai Jin – G. W. Woodruff School of Mechanical Engineering, Georgia Institute of Technology, Atlanta, Georgia 30332, United States

Michael J. Lee – G. W. Woodruff School of Mechanical Engineering, Georgia Institute of Technology, Atlanta, Georgia 30332, United States

Mochen Li – Department of Applied Chemistry, Waseda University, Tokyo 169-8555, Japan

Suguru Noda — Department of Applied Chemistry, Waseda University, Tokyo 169-8555, Japan; orcid.org/0000-0002-7305-5307

Complete contact information is available at: https://pubs.acs.org/10.1021/acsaem.0c00187

Author Contributions

[#]T.L., K.C.K. and B.L. equally contributed to this work. **Notes**

The authors declare no competing financial interest.

ACKNOWLEDGMENTS

B.L., K.C.K., and T.L. equally contributed to this work. This material is based upon the work supported by the National Science Foundation under Grant no. 1805052. This work was in part supported by the Basic Science Research Program through the National Research Foundation of Korea (NRF) funded by the Ministry of Science, ICT & Future Planning (NRF-2017R1C1B5017482). S.N. thanks the JSPS for Kakenhi Grant no. JP16H06368.

REFERENCES

- (1) Dunn, B.; Kamath, H.; Tarascon, J.-M. Electrical Energy Storage for the Grid: A Battery of Choices. *Science* **2011**, 334, 928–935.
- (2) Lee, S. W.; Gallant, B. M.; Byon, H. R.; Hammond, P. T.; Shao-Horn, Y. Nanostructured carbon-based electrodes: bridging the gap between thin-film lithium-ion batteries and electrochemical capacitors. *Energy Environ. Sci.* **2011**, *4*, 1972–1985.
- (3) Kolek, M.; Otteny, F.; Schmidt, P.; Mück-Lichtenfeld, C.; Einholz, C.; Becking, J.; Schleicher, E.; Winter, M.; Bieker, P.; Esser, B. Ultra-high cycling stability of poly(vinylphenothiazine) as a battery cathode material resulting from pi-pi interactions. *Energy Environ. Sci.* **2017**, *10*, 2334–2341.
- (4) Lee, S. W.; Yabuuchi, N.; Gallant, B. M.; Chen, S.; Kim, B.-S.; Hammond, P. T.; Shao-Horn, Y. High-power lithium batteries from functionalized carbon-nanotube electrodes. *Nat. Nanotechnol.* **2010**, *5*, 531–537.
- (5) Wu, Y.; Zeng, R.; Nan, J.; Shu, D.; Qiu, Y.; Chou, S.-L. Quinone Electrode Materials for Rechargeable Lithium/Sodium Ion Batteries. *Adv. Energy Mater.* **2017**, *7*, 1700278.
- (6) Hong, J.; Lee, M.; Lee, B.; Seo, D. H.; Park, C. B.; Kang, K. Biologically inspired pteridine redox centres for rechargeable batteries. *Nat. Commun.* **2014**, *5*, 5335.
- (7) Kim, K. C.; Liu, T.; Lee, S. W.; Jang, S. S. First-Principles Density Functional Theory Modeling of Li Binding: Thermodynamics and Redox Properties of Quinone Derivatives for Lithium-Ion Batteries. *J. Am. Chem. Soc.* **2016**, *138*, 2374–2382.
- (8) Liu, T.; Kim, K. C.; Lee, B.; Chen, Z.; Noda, S.; Jang, S. S.; Lee, S. W. Self-polymerized dopamine as an organic cathode for Li- and Na-ion batteries. *Energy Environ. Sci.* **2017**, *10*, 205–215.
- (9) Ma, T.; Zhao, Q.; Wang, J.; Pan, Z.; Chen, J. A Sulfur Heterocyclic Quinone Cathode and a Multifunctional Binder for a High-Performance Rechargeable Lithium-Ion Battery. *Angew. Chem., Int. Ed.* **2016**, *55*, 6428–6432.
- (10) Jaffe, A.; Saldivar Valdes, A.; Karunadasa, H. I. Quinone-Functionalized Carbon Black Cathodes for Lithium Batteries with High Power Densities. *Chem. Mater.* **2015**, 27, 3568–3571.
- (11) Chen, H.; Armand, M.; Demailly, G.; Dolhem, F.; Poizot, P.; Tarascon, J.-M. From biomass to a renewable LixC6O6 organic electrode for sustainable Li-ion batteries. *ChemSusChem* **2008**, *1*, 348–355.
- (12) Bachman, J. C.; Kavian, R.; Graham, D. J.; Kim, D. Y.; Noda, S.; Nocera, D. G.; Shao-Horn, Y.; Lee, S. W. Electrochemical polymerization of pyrene derivatives on functionalized carbon nanotubes for pseudocapacitive electrodes. *Nat. Commun.* **2015**, *6*, 7040
- (13) Shimizu, A.; Tsujii, Y.; Kuramoto, H.; Nokami, T.; Inatomi, Y.; Hojo, N.; Yoshida, J.-i. Nitrogen-Containing Polycyclic Quinones as Cathode Materials for Lithium-ion Batteries with Increased Voltage. *Energy Technol.* **2014**, *2*, 155–158.
- (14) Liu, K.; Zheng, J.; Zhong, G.; Yang, Y. Poly(2,5-dihydroxy-1,4-benzoquinonyl sulfide) (PDBS) as a cathode material for lithium ion batteries. *J. Mater. Chem.* **2011**, *21*, 4125–4131.
- (15) Han, X.; Chang, C.; Yuan, L.; Sun, T.; Sun, J. Aromatic Carbonyl Derivative Polymers as High-Performance Li-Ion Storage Materials. *Adv. Mater.* **2007**, *19*, 1616–1621.
- (16) Ismail, K. M.; Khalifa, Z. M.; Azzem, M. A.; Badawy, W. A. Electrochemical preparation and characterization of poly (1-amino-9, 10-anthraquinone) films. *Electrochim. Acta* **2002**, *47*, 1867–1873.
- (17) Badawy, W. A.; Ismail, K. M.; Medany, S. S. Kinetics of electropolymerization of 1-amino-9, 10-anthraquinone. *Int. J. Chem. Kinet.* **2011**, *43*, 141–146.
- (18) Admassie, S.; Elfwing, A.; Inganäs, O. Electrochemical synthesis and characterization of interpenetrating networks of conducting polymers for enhanced charge storage. *Adv. Mater. Interfaces* **2016**, *3*, 1500533.
- (19) Liu, J.; Liu, P. Well-defined poly (1, 5-diaminoanthraquinone)/reduced graphene oxide hybrids with superior electrochemical property for high performance electrochemical capacitors. *J. Colloid Interface Sci.* **2019**, 542, 33–44.

- (20) Liu, J.; Wang, Q.; Liu, P. Poly (1, 5-diaminoanthraquinone) coated carbon cloth composites as flexible electrode with extraordinary cycling stability for symmetric solid-state supercapacitors. *J. Colloid Interface Sci.* **2019**, *546*, 60–69.
- (21) Xu, G.; Lu, Q.; Wen, L.; Liu, G.; Ci, Y. Poly (1, 5-diaminoanthraquinone) as cathode material in rechargeable lithium batteries. *Acta Polym. Sin.* **2010**, *6*, 795.
- (22) Paulson, S. C.; Sapp, S. A.; Elliott, C. M. Electrochemical and spectroelectrochemical investigations into the nature of charge-trapping in electrochemically-generated homopolymer films of tris(4-vinyl-4 '-methyl-2,2 '-bipyridine)ruthenium(II). *J. Phys. Chem. B* **2001**, *105*, 8718–8724.
- (23) Algharaibeh, Z.; Pickup, P. G. Charge trapping in poly(1-amino-anthraquinone) films. *Electrochim. Acta* **2013**, 93, 87–92.
- (24) Borjas, R.; Buttry, D. A. EQCM studies of film growth, redox cycling, and charge trapping of n-doped and p-doped poly-(thiophene). *Chem. Mater.* **1991**, *3*, 872–878.
- (25) Denisevich, P.; Willman, K. W.; Murray, R. W. Unidirectional current flow and charge state trapping at redox polymer interfaces on bilayer electrodes: principles, experimental demonstration, and theory. *J. Am. Chem. Soc.* **1981**, 103, 4727–4737.
- (26) Zhang, H.; Yao, M.; Wei, J.; Zhang, Y.; Zhang, S.; Gao, Y.; Li, J.; Lu, P.; Yang, B.; Ma, Y. Stable p/n-Dopable Conducting Redox Polymers for High-Voltage Pseudocapacitor Electrode Materials: Structure-Performance Relationship and Detailed Investigation into Charge-Trapping Effect. *Adv. Energy Mater.* **2017**, *7*, 1701063.
- (27) Lee, S. W.; Gallant, B. M.; Lee, Y.; Yoshida, N.; Kim, D. Y.; Yamada, Y.; Noda, S.; Yamada, A.; Shao-Horn, Y. Self-standing positive electrodes of oxidized few-walled carbon nanotubes for light-weight and high-power lithium batteries. *Energy Environ. Sci.* **2012**, *5*, 5437–5444.
- (28) Kim, D. Y.; Sugime, H.; Hasegawa, K.; Osawa, T.; Noda, S. Sub-millimeter-long carbon nanotubes repeatedly grown on and separated from ceramic beads in a single fluidized bed reactor. *Carbon* **2011**, *49*, 1972–1979.
- (29) Sieuw, L.; Jouhara, A.; Quarez, É.; Auger, C.; Gohy, J.-F.; Poizot, P.; Vlad, A. A H-bond stabilized quinone electrode material for Li-organic batteries: the strength of weak bonds. *Chem. Sci.* **2019**, 10, 418–426.
- (30) Gospodinova, N.; Terlemezyan, L. Conducting polymers prepared by oxidative polymerization: Polyaniline. *Prog. Polym. Sci.* **1998**, 23, 1443–1484.
- (31) Naoi, K.; Suematsu, S.; Manago, A. Electrochemistry of poly(1,5-diaminoanthraquinone) and its application in electrochemical capacitor materials. *J. Electrochem. Soc.* **2000**, 147, 420–426.
- (32) Mamtani, K.; Jain, D.; Zemlyanov, D.; Celik, G.; Luthman, J.; Renkes, G.; Co, A. C.; Ozkan, U. S. Probing the Oxygen Reduction Reaction Active Sites over Nitrogen-Doped Carbon Nanostructures (CNx) in Acidic Media Using Phosphate Anion. ACS Catal. 2016, 6, 7249–7259.
- (33) Kim, H.; Kwon, J. E.; Lee, B.; Hong, J.; Lee, M.; Park, S. Y.; Kang, K. High Energy Organic Cathode for Sodium Rechargeable Batteries. *Chem. Mater.* **2015**, *27*, 7258–7264.
- (34) Zhu, Y.; Kim, K. C.; Jang, S. S. Boron-doped coronenes with high redox potential for organic positive electrodes in lithi-um-ion batteries: a first-principles density functional theory modeling study. *J. Mater. Chem. A* **2018**, *6*, 10111–10120.
- (35) Kang, J.; Kim, K. C.; Jang, S. S. Density functional theory modeling assisted investigation of thermodynamics and redox properties of boron-doped corannulenes for cathodes in lithium-ion batteries. *J. Phys. Chem. C* **2018**, *122*, 10675–10681.
- (36) Liu, T.; Kim, K. C.; Kavian, R.; Jang, S. S.; Lee, S. W. High-Density Lithium-Ion Energy Storage Utilizing the Surface Redox Reactions in Folded Graphene Films. *Chem. Mater.* **2015**, 27, 3291–3298.
- (37) Park, J. H.; Liu, T.; Kim, K. C.; Lee, S. W.; Jang, S. S. Systematic Molecular Design of Ketone Derivatives of Aromatic Molecules for Lithium-Ion Batteries: First-Principles DFT Modeling. *ChemSusChem* **2017**, *10*, 1584–1591.

- (38) Kim, S.; Kim, K. C.; Lee, S. W.; Jang, S. S. Thermodynamic and redox properties of graphene oxides for lithium-ion battery applications: a first principles density functional theory modeling approach. *Phys. Chem. Chem. phys.* **2016**, *18*, 20600–20606.
- (39) Snook, G. A.; Kao, P.; Best, A. S. Conducting-polymer-based supercapacitor devices and electrodes. *J. Power Sources* **2011**, *196*, 1–12.

Supporting Information

Enhanced Lithium Storage of an Organic Cathode via Bipolar Mechanism

Tianyuan Liu, \S , \dagger Ki Chul Kim, \ddagger , \dagger Byeongyong Lee, \S , \dagger Shikai Jin, \S Michael J. Lee, \S Mochen Li, \dagger Suguru Noda, \dagger Seung Soon Jang \dagger , \ast and Seung Woo Lee \S , \ast

§G. W. Woodruff School of Mechanical Engineering, Georgia Institute of Technology, Atlanta, GA 30332, USA

[‡]Division of Chemical Engineering, Konkuk University, Seoul 05029, The Republic of Korea [‡]Department of Applied Chemistry, Waseda University, Tokyo 169-8555, Japan [‡]Computational NanoBio Technology Laboratory, School of Materials Science and Engineering, Georgia Institute of Technology, Atlanta, GA 30332, USA

Corresponding Authors: seung.lee@me.gatech.edu, seung.lee@me.gatech.edu, seung.lee@me.gatech.edu, seung.lee@me.gatech.edu, seung.lee@me.gatech.edu, seung.lee@me.gatech.edu, seung.lee@mse.gatech.edu, seung.lee@mse.gatech.edu, seung.lee@mse.gatech.edu, seung.seungsoon.jang@mse.gatech.edu, seung.seungsoon.jang@mse.gatech.edu, seung.seungsoon.jang@mse.gatech.edu, seung.seungsoon.jang@mse.gatech.edu, seungsoon.jang@mse.gatech.edu, seungsoon.jang@mse.gatech.edu,

[†]These authors equally contributed to this work.

Experimental Methods

Chemical: All the organic molecules, p-benzoquinone (≥98%, BQ), 1,4-naphthoquinone (97%, NQ), anthraquinone (97%, AQ), 1-aminoanthraquinone (97%), and 1,5-diaminoanthraquinone (85%) were purchased from Sigma Aldrich, and used without further purification.

Electrode preparation: Aqueous mixtures (15 mL) of FWNTs (3.3 mg) and organic molecules at varied mass ratios (1:1 or 1:2) were sonicated overnight. Then, the mixtures were vacuum filtered using a piece of Celgard 3501 separator. Flexible and free-standing films were finally obtained through further vacuum drying process. Pristine FWNT films were obtained following similar process without adding any organic molecules. The weight percentage of organic molecule in the hybrid film was calculated by measuring the relative change in the mass of the composite film compared to the pristine FWNT.

Characterization: Characterization of microstructures and morphologies was conducted by a scanning electron microscope (SEM) (Hitachi SU8010, operated at 5 kV). Raman spectra were collected by Thermo Nicolet Almega XR Dispersive Raman Spectrometer using a 488-nm wavelength laser. Chemical analysis was conducted by X-ray photoelectron spectroscopy (XPS, Thermal Scientific K-alpha XPS instrument). High-resolution C1s peaks were fitted using XPSPEAKS 4.1 software.

Electrochemical measurements: Electrochemical properties of the hybrid films were measured using two-electrode type Swagelok cells and LIR2032 coin cells, where a piece of Li foil (anode) and a piece of hybrid film (cathode) were separated by two pieces of Celgard 2500 separator. The electrolyte used in the cells was 1 M LiPF₆ in a mixture of ethylene carbonate (EC) and dimethyl carbonate (DMC) (3:7 V/V, BASF). All the cells were assembled in an Ar filled glovebox (MBraun). The mass loading of the hybrid films was in the range of 1–4 mg/cm². Cyclic voltammetry and galvanostatic charge/discharge testswere carried out using a Bio-Logic VMP3 potentiostat/galvanostat, and extended cycling test was done using an Arbin LBT-21084, both at room temperature. The capacity of the electrode was calculated based on the mass of the active material (AAQ/DAAQ). The voltage window of the cells was kept at 1.5–4.5 V vs. Li.

Density functional theory (DFT) calculations: All the DFT calculations were performed using the Jaguar program with a 6-31+G(d,p) basis set.¹ The PBE0 level of theory was chosen to geometrically optimize AAQ and DAAQ monomers and their dimers with or without the binding

of charge carrier(s), namely Li and PF6.² The vibrational frequency calculations with the same level of theory and basis set were further carried out using Poisson-Boltzmann implicit solvation model to approximate the solvation contributions to the free energies of the molecules at 298 K in vacuum.³ A dielectric constant of 16.14, which reliably describes the polarity of the solvents in mixture in our systems, was used for the solvation free energy calculations.

The thermodynamic cycle described elsewhere was used to predict the redox potentials of the molecules.⁴⁻¹¹ The redox potential (ΔE^{red}) of a molecule in solution with respect to a Li reference electrode can be predicted by

$$\Delta E^{red} = \frac{-\Delta G^{soln}}{nF} - 1.39 V \tag{1}$$

where, ΔG^{soln} is the difference in the Gibbs free energy in solution during the reduction, n is the number of electrons transferred, and F is the Faraday constant. The constant, 1.39 V, indicates the redox potential of the Li/Li⁺ reference electrode. The electronic properties, such as electron affinity and frontier orbitals (i.e., the highest occupied molecular orbital (HOMO) and LUMO energy levels) of targeted molecules were further examined to correlate them with the redox potential.

The DFT calculations with the afore-mentioned level of theory and basis set were performed to predict potential energy surfaces for Li escaping from AAQ and DAAQ monomers in cathodes during the recharging process. For each of the monomers, we performed the relaxed scanning process dragging out Li from its most stable binding configuration with the aim of identifying the activation energy barrier of the Li diffusion process.

Table S1. The calculated redox potentials for AAQ and DAAQ monomers with/without bound Li atom(s) and their electronic properties, namely electron affinity, HOMO, and LUMO.

Monomer	Calculated Redox Potential (V)	Electron Affinity (kcal/mol)	HOMO (eV)	LUMO (eV)	HOMO-LUMO gap (eV)
AAQ	2.12	-38.1	-6.33	-2.85	3.48
AAQ-Li	1.57	-29.6	-4.91	-1.94	2.97
AAQ-2Li	-0.76	-19.5	-3.95	-1.44	2.51
DAAQ	1.95	-35.0	-6.09	-2.68	3.41
DAAQ-Li	1.48	-28.0	-4.86	-1.75	3.11
DAAQ-2Li	-1.36	-9.1	-3.77	-0.88	2.89

Table S2. The calculated redox potentials for AAQ and DAAQ dimers with/without bound electrolyte ion(s), namely Li and PF₆. Their electronic properties, namely electron affinity, HOMO, and LUMO, are also listed in the table.

Dimer	Calculated Redox	Electron	НОМО	LUMO	HOMO-LUMO
	Potential	Affinity	(eV)	(eV)	gap (eV)
	(V)	(kcal/mol)			
$(AAQ)_2$	2.16	-47.8	-5.69	-2.96	2.73
(AAQ) ₂ -Li	1.98	-56.1	-4.99	-3.05	1.94
(AAQ) ₂ -2Li	1.83	-49.6	-3.92	-2.82	1.10
(AAQ) ₂ -3Li	1.32	-38.8	-3.67	-1.94	1.73
(AAQ) ₂ -4Li	0.59	-18.6	-3.84	-1.25	2.59
(AAQ) ₂ -PF ₆	3.94	-103.8	7.18	-4.20	2.98
(DAAQ) ₂	2.08	-46.5	-5.69	-2.89	2.80
(DAAQ) ₂ -Li	1.93	-44.7	-5.02	-2.71	2.31
(DAAQ) ₂ -2Li	1.50	-33.5	-4.06	-2.10	1.96
(DAAQ) ₂ -3Li	1.37	-32.5	-3.59	-1.80	1.79
(DAAQ) ₂ -4Li	-0.39	-30.5	-3.73	-1.32	2.41
(DAAQ) ₂ -PF ₆	3.82	-96.3	-6.37	-4.33	2.04
(DAAQ) ₂ -2PF ₆	4.51	-128.1	-8.00	-5.44	2.56

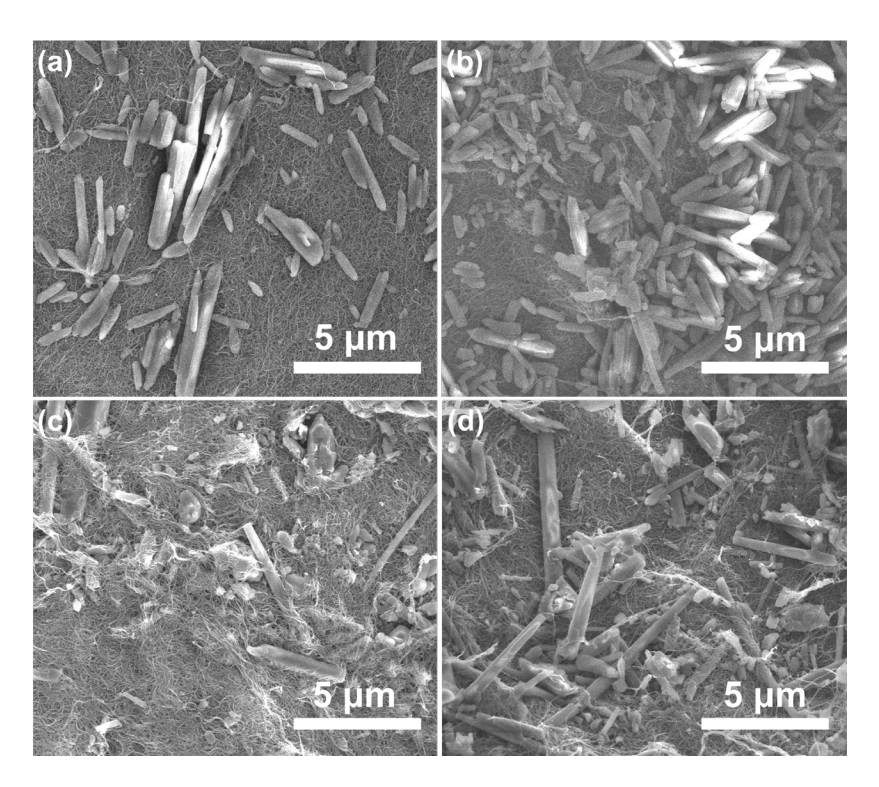


Figure S1. Scanning electron microscope (SEM) images of composite films consisting of (a, b) FWNTs and 1-aminoanthraquinone (AAQ-NT), (c, d) FWNTs and 1, 5-diaminoanthraquinone (DAAQ-NT). The mass ratios between molecules and FWNTs are 1:1 in (a, c), and 2:1 in (b, d).

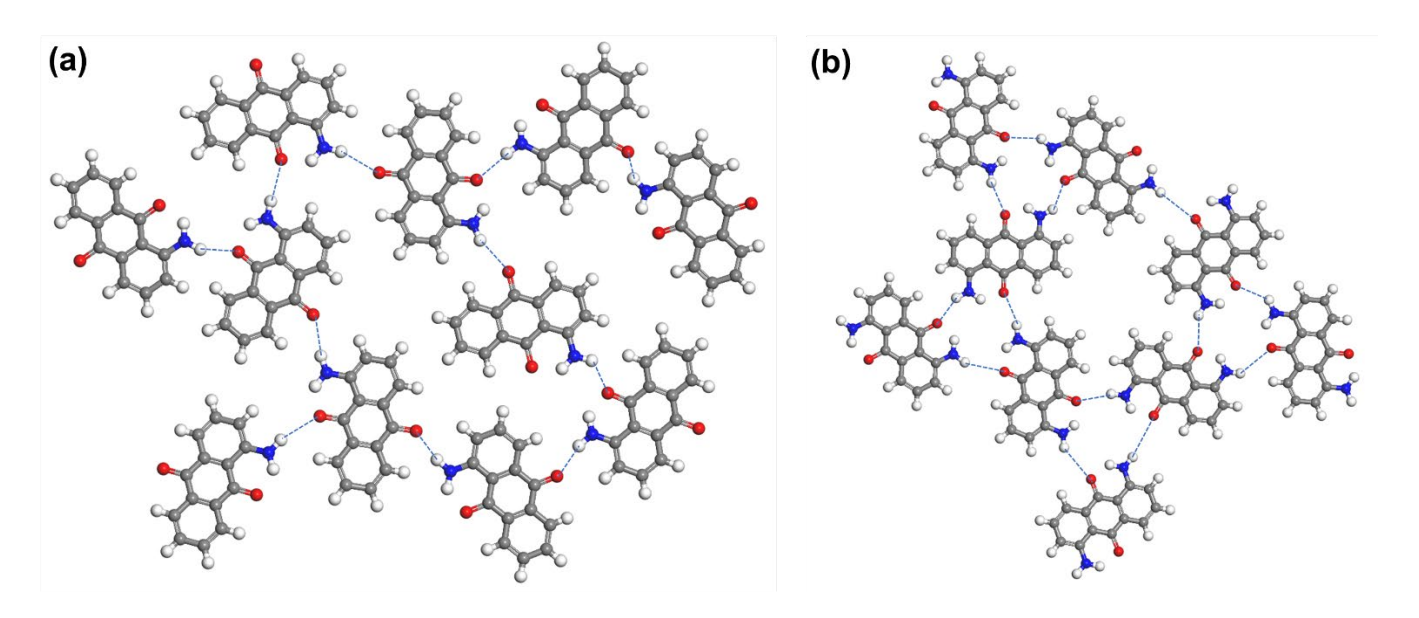


Figure S2. Schematic illustrations of feasible hydrogen bonding networks for (a) AAQ and (b) DAAQ.

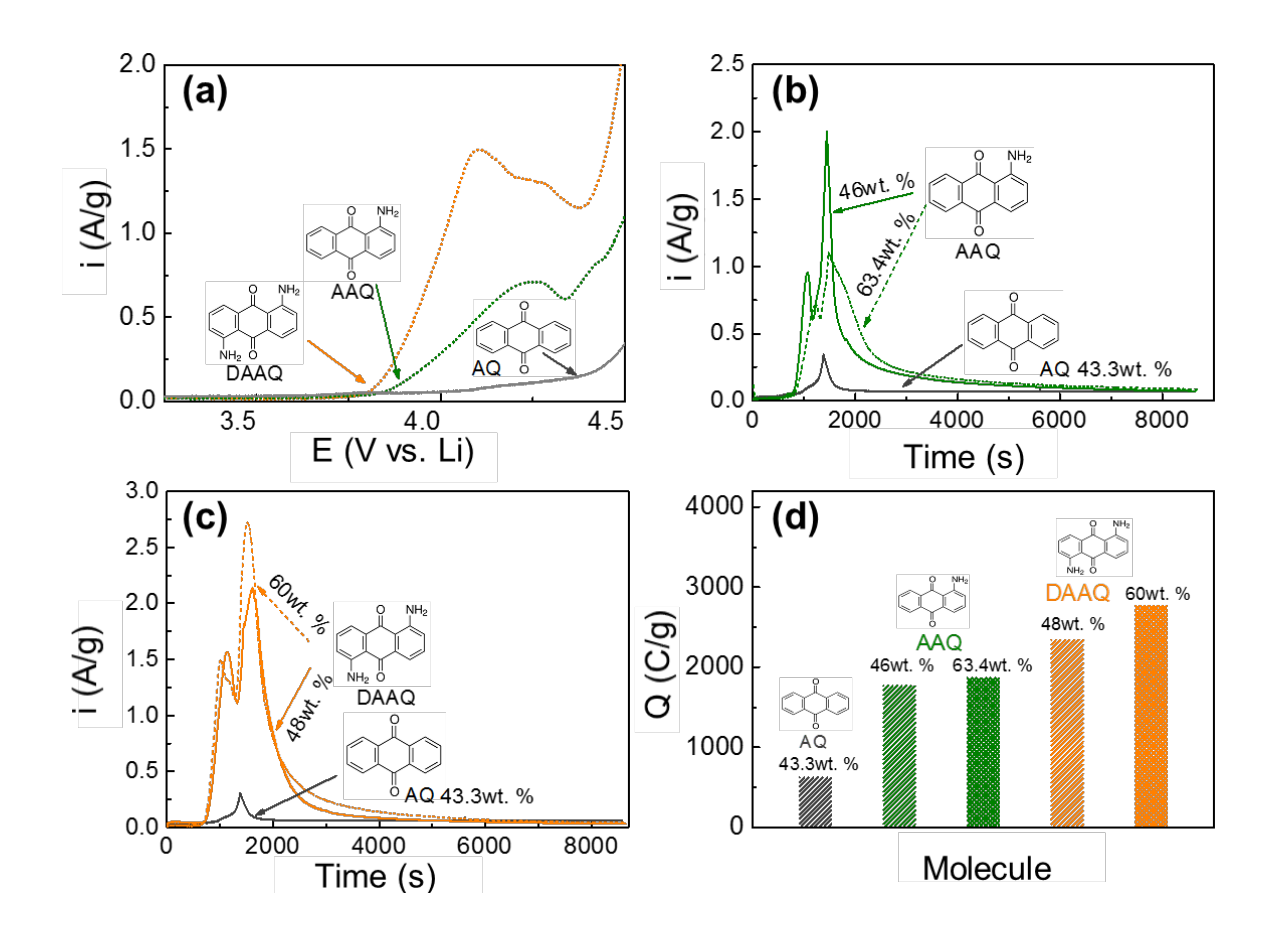


Figure S3. (a) Linear sweep voltammetry (LSV) measurements for AAQ-NT and DAAQ-NT hybrid films with AAQ (63.4 wt.%) and DAAQ (60 wt.%) loadings, respectively, from open circuit voltage to 4.5 V vs. Li at a scan rate of 1 mV/s. The anodic current as a function of time during the LSV measurements followed by a 2-hour potentiostatic polymerization process at the fixed voltage of 4.5 V vs. Li for (b) AAQ-NT and (c) DAAQ-NT hybrid films with varied monomer loadings. (d) Charges transferred during the LSV followed by the 2-hour potentiostatic polymerization process for AAQ-NT and DAAQ-NT hybrid films with varied monomer loadings. Resultant values for AQ-NT hybrid films are shown as reference in all the figures. All the electrochemical measurements were conducted in a two-electrode Swagelok-type cell with a piece of Li metal as a counter electrode.

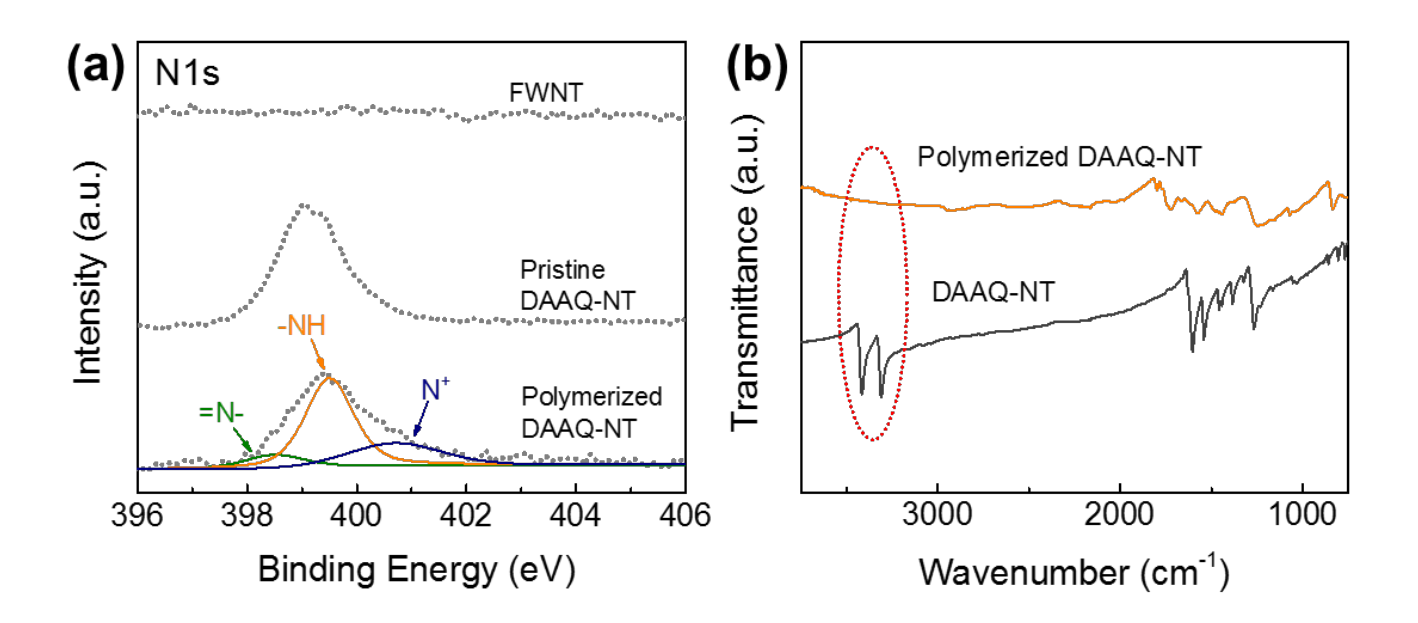


Figure S4. (a) High resolution XPS spectra of N1s peak for pristine FWNT, DAAQ-NT, and electrochemically-polymerized poly-DAAQ-NT films. (b) Fourier transform infrared (FTIR) spectroscopy of DAAQ-NT and electrochemically-polymerized poly-DAAQ-NT films.

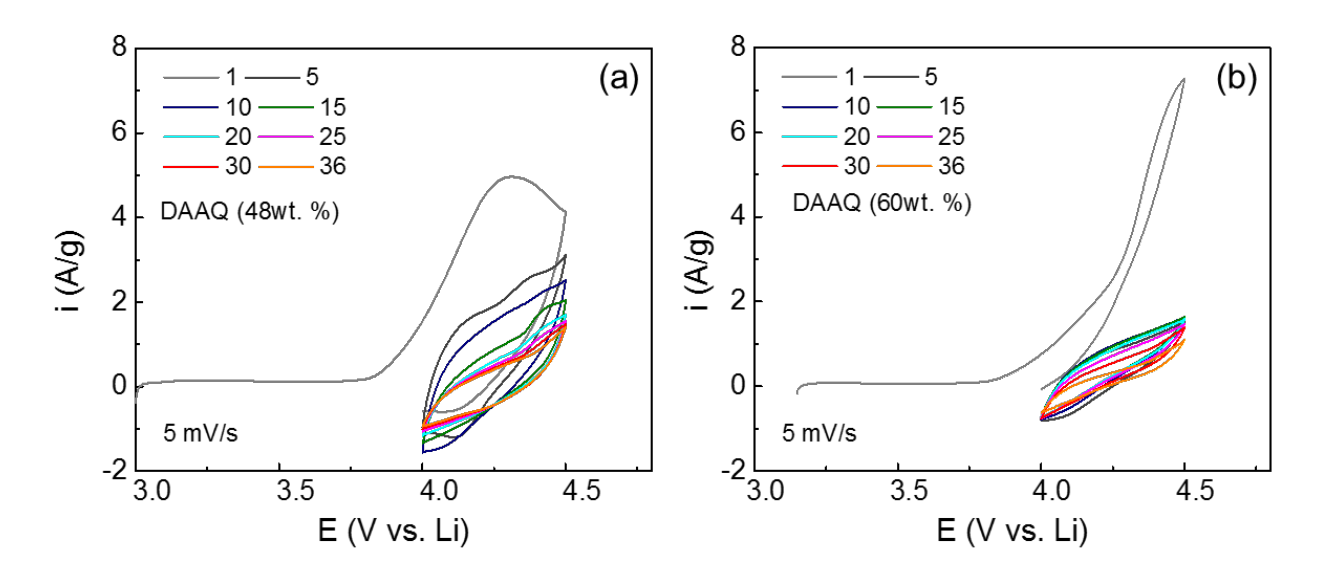


Figure S5. CV scans of the potentiodynamic polymerization process of (a) DAAQ (48 wt.%) and (b) DAAQ (60 wt.%) measured within the voltage window of 4.0 – 4.5 V vs. Li at a scan rate of 5 mV/s for 36 cycles.

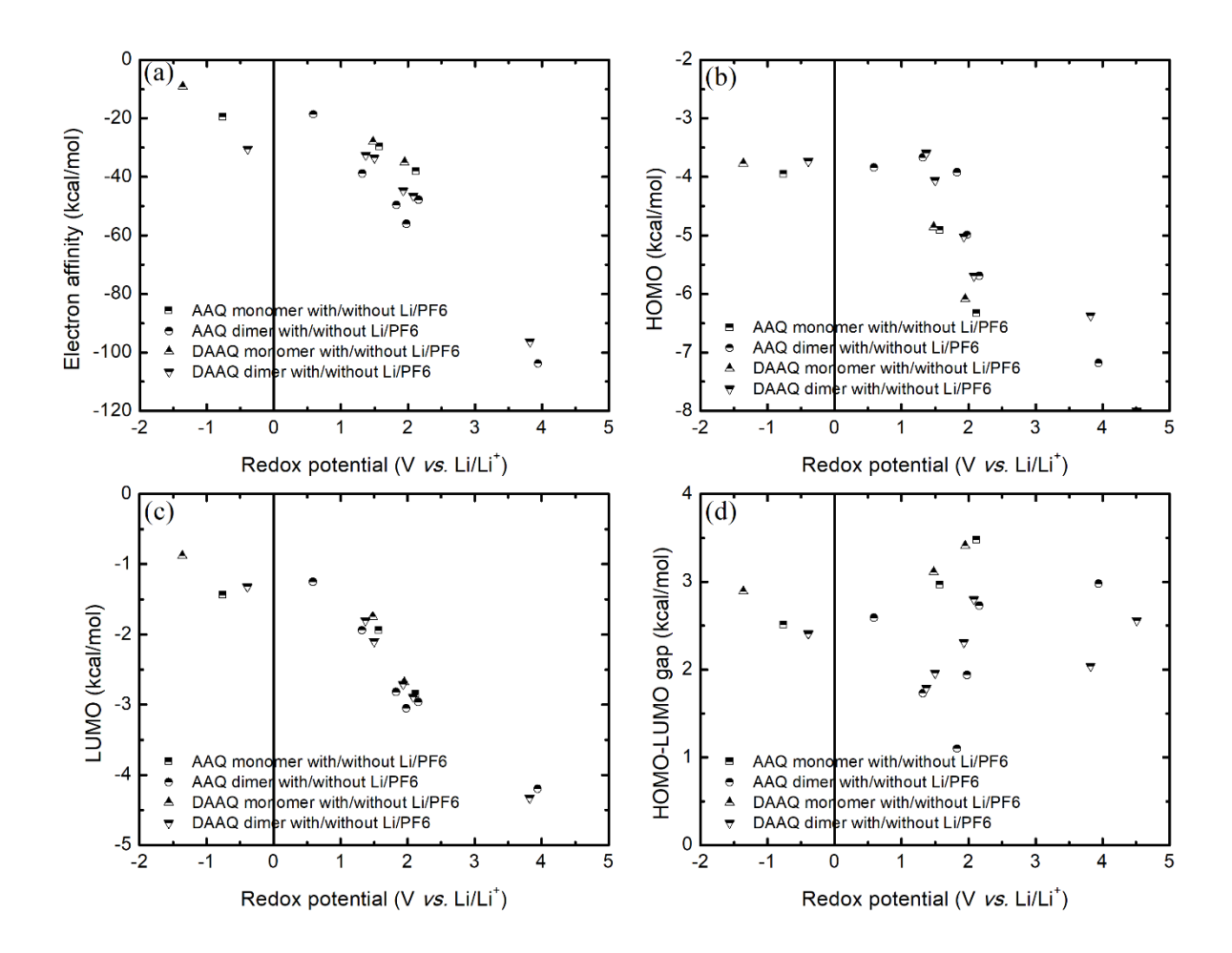


Figure S6. The calculated redox potentials of AAQ and DAAQ monomers and their dimers with/without bound Li/PF₆ ions to be correlated with their electronic properties, namely (a) electron affinity, (b) HOMO, (c) LUMO, and (d) HOMO-LUMO gap.

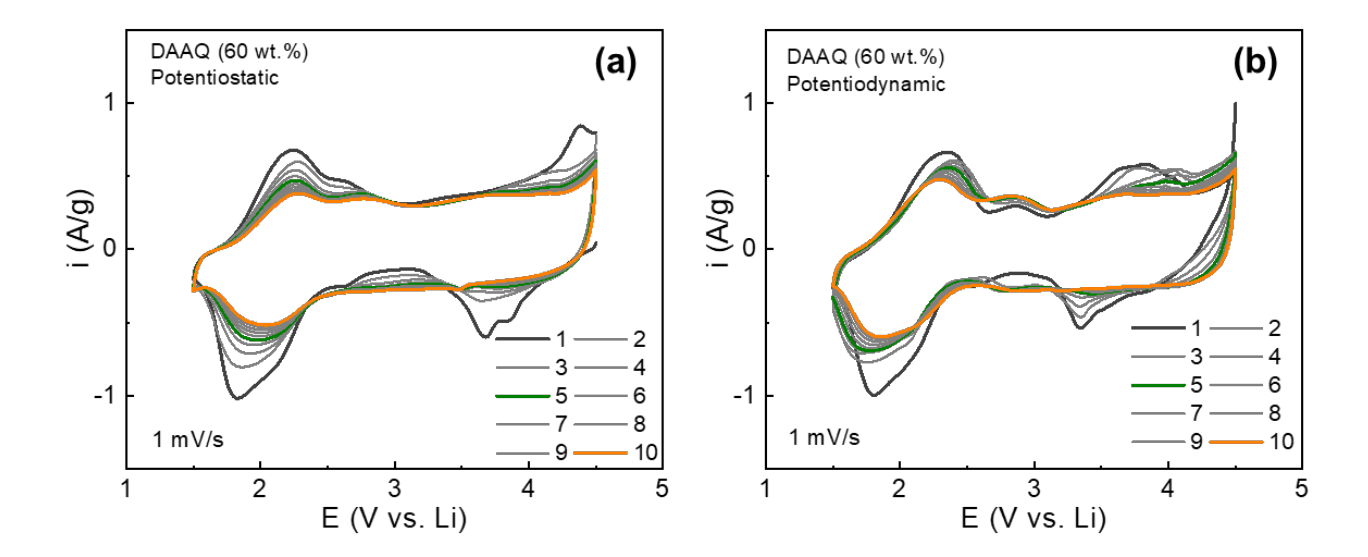


Figure S7. CV scans for hybrid films containing (a) potentiostatically- and (b) potentiodynamically-polymerized DAAQ with 60 wt.% measured within the voltage window of 1.5 - 4.5 V vs. Li at a scan rate of 1 mV/s for 10 cycles.

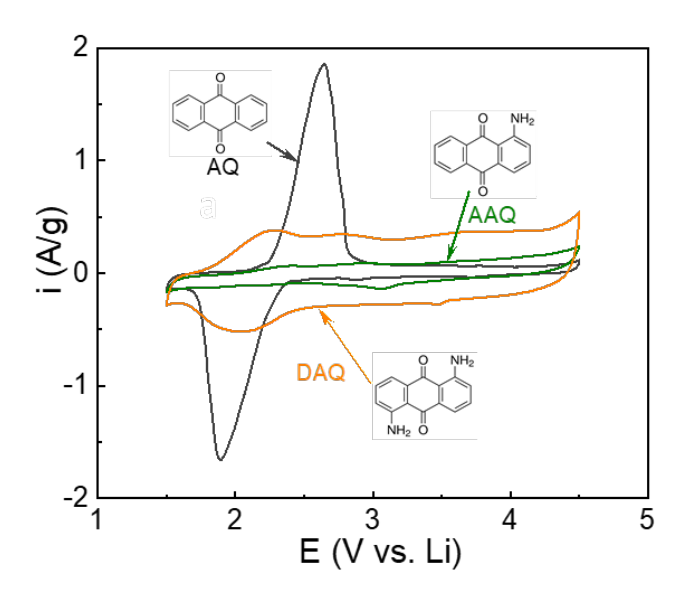


Figure S8. Cyclic voltammetry (CV) measurement of the potentiostatically polymerized hybrid films for AQ, AAQ and DAAQ.

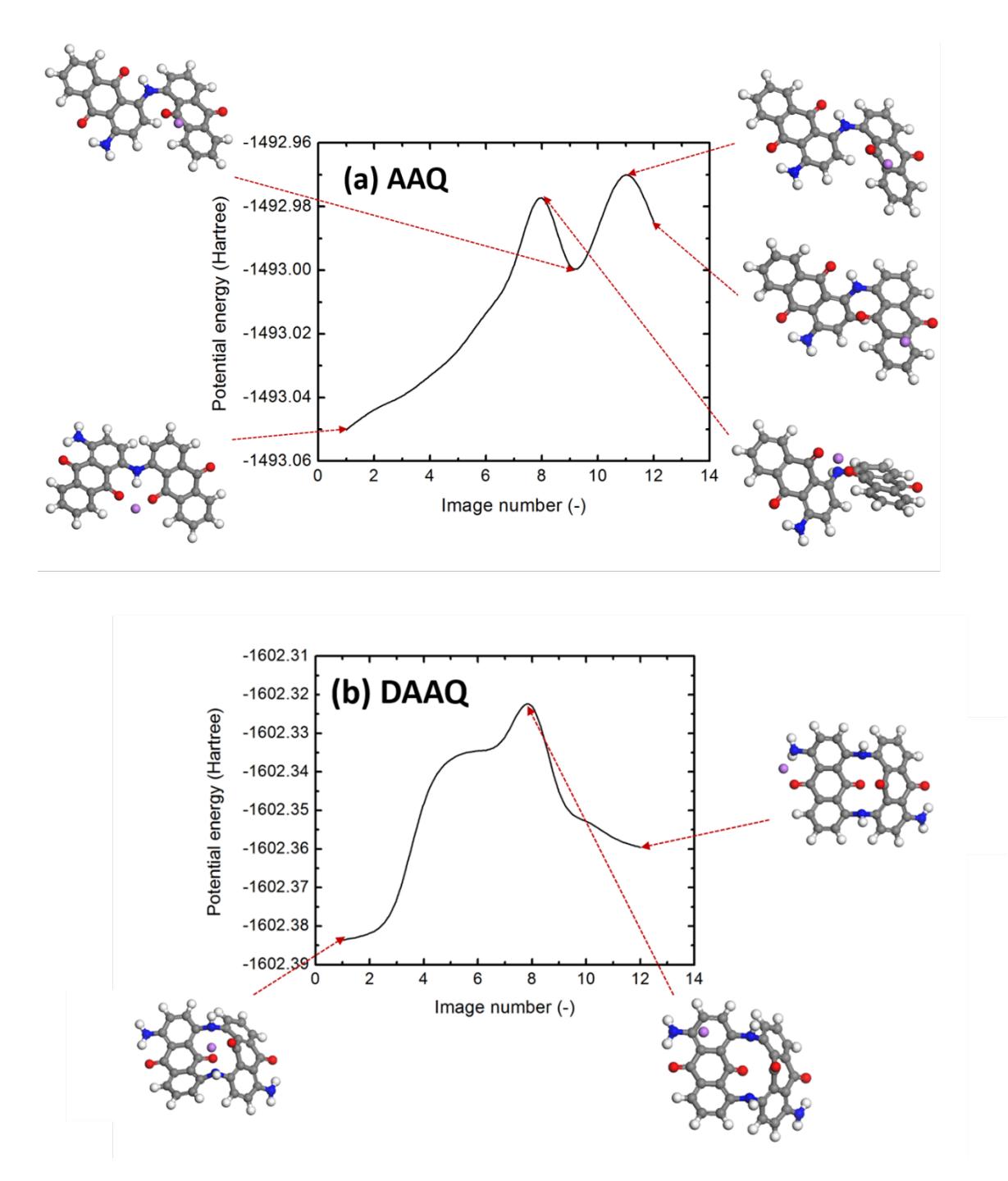


Figure S9. The potential energy surfaces for Li diffusing through (a) AAQ and (b) DAAQ during the recharging process. The structural changes of the organic molecules induced by the Li-diffusion process are visualized along the potential energy surface profiles.

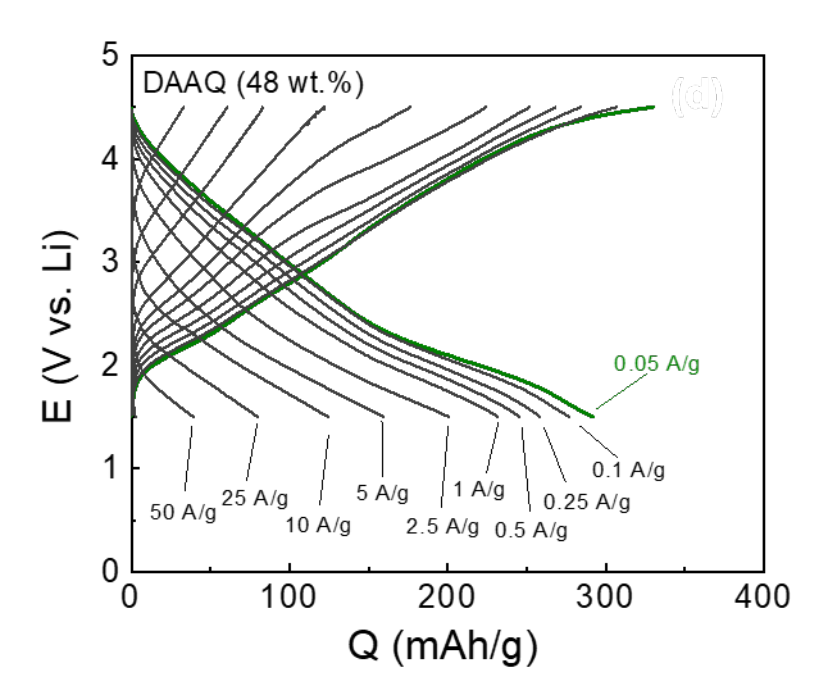


Figure S10. Rate-dependent galvanostatic charge and discharge profiles for poly-DAAQ-NT films with DAAQ loading of 48 wt.%. The electrode was potentiodynamically polymerized within the voltage window of 4.0 - 4.5 V vs. Li at a scan rate of 5 mV/s for 108 cycles.

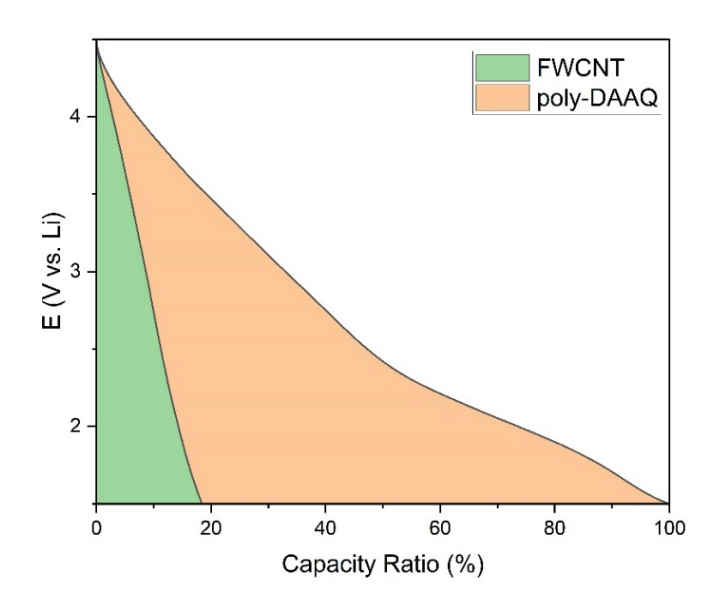


Figure S11. Capacity contribution of FWCNT and potentiodynamically polymerized DAAQ for the poly-DAAQ-NT film electrode with a DAAQ loading of 60 wt.% at 0.05 A/g.

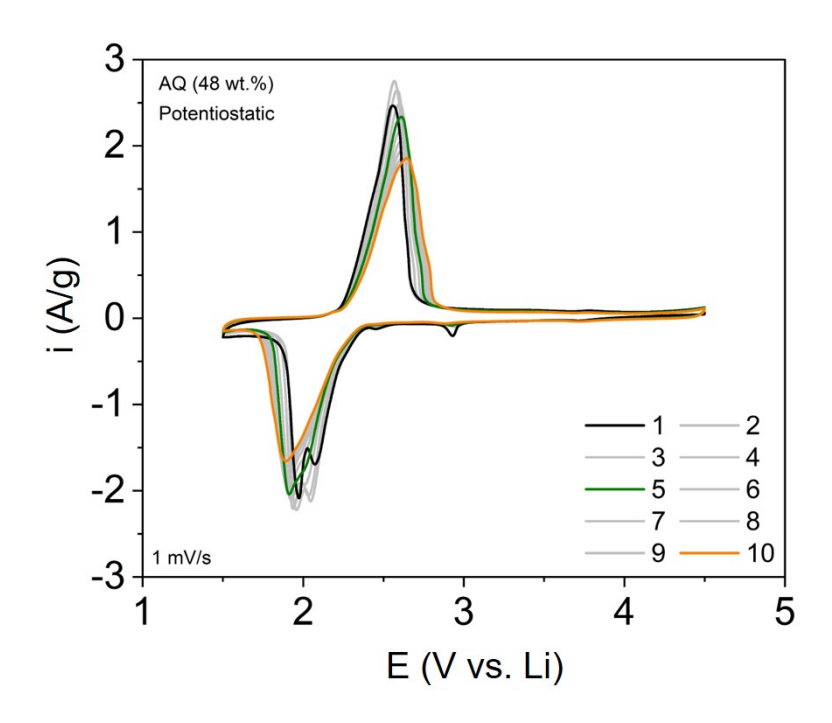


Figure S12. Cyclic voltammetry scans for AQ-NT film (48 wt.%) after the potentiostatic polymerization at 1mV/s.

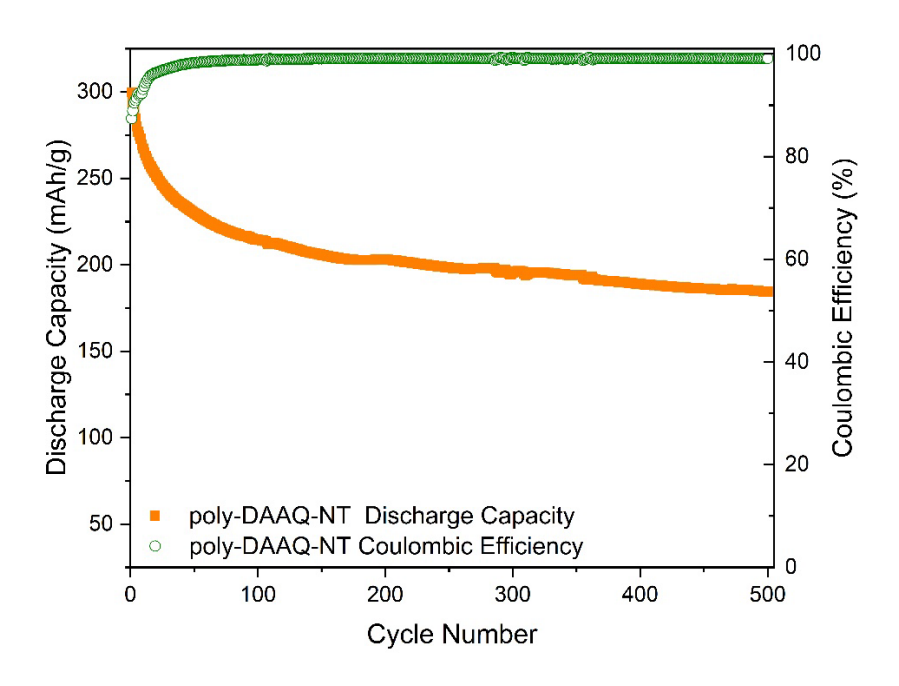


Figure S13. Extended cycling testing of the poly-DAAQ hybrid film (60 wt.%) at 1 A/g for 500 cycles.

Table S3 Comparison of electrochemical performances of various organic electrodes.

	Capacity	v ^a (mAh/g)		Ref#
Material	Low Current Density (0.05-0.1 A/g)	High Current Density (~5 A/g)	Cycling Stability	
poly(anthraquinonyl sulfide)/graphene	187 (Li)	136 (Li)	NA	12
polyimide/graphene	205 (Li)	80 (Li)	NA	12
poly(anthraquinonyl sulfide)	198 (Li)	161 (0.5 A/g)	NA	13
Polyimide/SWNT	226 (Li)	160	85% (100 cycles)	14
lithium 2,6-bis(ethoxycarbonyl)-3,7-dioxo-3,7-dihydro-s-indacene-1,5-bis(olate)	125 (Li)	NA	NA	15
benzofuro[5,6-b]furan-4,8-dione benzo[1,2-b:4,5-b']dithiophene-4,8- dione pyrido[3,4-g]isoquinoline-5,10-dione	208–234 (Li)	NA	65% after 100 cycles 86% after 100 cycles 80% after 100 cycles	16
Li ₄ C ₈ H ₂ O ₆	223 (Li)	145 (1.2 A/g)	94% after 50 cycles	17
lithium salt of poly(2,5-dihydroxy-p-benzoquinonyl sulfide)	247(Li)	207	90% after 1500 cycles (relative to the second cycle)	18
Polydopamine/FWNT	217-235 (Li)	111-149 (Li)	100.7% after 10,000 cycles	9
poly(1,4-anthraquinone) poly(1,5-anthraquinone)	250 (Li) 235	180 100	99% after 1000 cycles	19
Lumiflavine/SWNT	200(Li)	155	100% after 100 cycles	20
9,10-anthraquinone/SWNT 9,10-phenanthrenequinone/SWNT	255(Li) 280	NA	37% after 50 cycles 47% after 50 cycles	21
poly(2,5-dihydroxyl-1,4- benzoquinonyl sulfide)/SWNT	200 (Li)	80	89% after 500 cycles	22
1,3,5-tris(4- formylphenyl)benzene/2,6- diaminoanthraquinone COF	225 (Li)	100 (3A/g)	86% after 1800 cycles	23
poly(benzo[1,2-b:4,5-b']dithiophene-4,8-dione-2,6-diyl/CNT	205 (Li)	155	96% after 250 cycles	24
Polyimide from PTCDA and DAAQ	128 (Li)	70	70% after 280 cycles	25
1,5-diaminoanthraquinone/FWNT	277-311 (Li)	197	83% after 100 cycles	This work

a) Specific capacity was calculated based on mass of active material.

References

- (1) Jaguar version 7.6, Schrodinger, LLC: New York, NY, 2009.
- (2) Adamo, C.; Barone, V., Accurate excitation energies from time-dependent density functional theory: assessing the PBE0 model for organic free radicals. *Chem. Phys. Lett.* **1999**, *314*, 152-157.
- (3) Tannor, D. J.; Marten, B.; Murphy, R.; Friesner, R. A.; Sitkoff, D.; Nicholls, A.; Honig, B.; Ringnalda, M.; Goddard, W. A., Accurate First Principles Calculation of Molecular Charge Distributions and Solvation Energies from Ab Initio Quantum Mechanics and Continuum Dielectric Theory. *J. Am. Chem. Soc.* **1994**, *116*, 11875-11882.
- (4) Winget, P.; Cramer, C. J.; Truhlar, D. G., Computation of equilibrium oxidation and reduction potentials for reversible and dissociative electron-transfer reactions in solution. *Theor. Chem. Acc.* **2004**, *112*, 217-227.
- (5) Zhu, Y.; Kim, K. C.; Jang, S. S., Boron-doped coronenes with high redox potential for organic positive electrodes in lithi-um-ion batteries: a first-principles density functional theory modeling study. *J. Mater. Chem. A* **2018**, *6*, 10111-10120.
- (6) Kang, J.; Kim, K. C.; Jang, S. S., Density functional theory modeling assisted investigation of thermodynamics and redox properties of boron-doped corannulenes for cathodes in lithium-ion batteries. *J. Phys. Chem. C* **2018**, *122*, 10675-10681.
- (7) Kim, K. C.; Liu, T.; Lee, S. W.; Jang, S. S., First-Principles Density Functional Theory Modeling of Li Binding: Thermodynamics and Redox Properties of Quinone Derivatives for Lithium-Ion Batteries. *J. Am. Chem. Soc.* **2016**, *138*, 2374-2382.
- (8) Liu, T.; Kim, K. C.; Kavian, R.; Jang, S. S.; Lee, S. W., High-Density Lithium-Ion Energy Storage Utilizing the Surface Redox Reactions in Folded Graphene Films. *Chem. Mater.* **2015**, *27*, 3291-3298.
- (9) Liu, T.; Kim, K. C.; Lee, B.; Chen, Z.; Noda, S.; Jang, S. S.; Lee, S. W., Self-polymerized dopamine as an organic cathode for Li- and Na-ion batteries. *Energy Environ. Sci.* **2017**, *10*, 205-215.
- (10) Park, J. H.; Liu, T.; Kim, K. C.; Lee, S. W.; Jang, S. S., Systematic Molecular Design of Ketone Derivatives of Aromatic Molecules for Lithium-Ion Batteries: First-Principles DFT Modeling. *ChemSusChem* **2017**, *10*, 1584-1591.
- (11) Kim, S. H.; Kim, K. C.; Lee, S. W.; Jang, S. S., Thermodynamic and redox properties of graphene oxides for lithium-ion battery applications: a first principles density functional theory modeling approach. *Phys. Chem. Chem. phys.* **2016**, *18*, 20600-20606.
- (12) Song, Z. P.; Xu, T.; Gordin, M. L.; Jiang, Y. B.; Bae, I. T.; Xiao, Q. F.; Zhan, H.; Liu, J.; Wang, D. H., Polymer-Graphene Nanocomposites as Ultrafast-Charge and -Discharge Cathodes for Rechargeable Lithium Batteries. *Nano Lett.* **2012**, *12*, 2205-2211.

- (13) Song, Z. P.; Zhan, H.; Zhou, Y. H., Anthraquinone based polymer as high performance cathode material for rechargeable lithium batteries. *Chem. Commun.* **2009**, 4, 448-450.
- (14) Wu, H. P.; Shevlin, S. A.; Meng, Q. H.; Guo, W.; Meng, Y. N.; Lu, K.; Wei, Z. X.; Guo, Z. X., Flexible and Binder-Free Organic Cathode for High-Performance Lithium-Ion Batteries. *Adv. Mater.* **2014**, *26*, 3338-3343.
- (15) Walker, W.; Grugeon, S.; Mentre, O.; Laruelle, S.; Tarascon, J. M.; Wudl, F., Ethoxycarbonyl-Based Organic Electrode for Li-Batteries. *J. Am. Chem. Soc.* **2010**, *132*, 6517-6523.
- (16) Liang, Y. L.; Zhang, P.; Yang, S. Q.; Tao, Z. L.; Chen, J., Fused Heteroaromatic Organic Compounds for High-Power Electrodes of Rechargeable Lithium Batteries. *Adv. Energy Mater.* **2013**, *3*, 600-605.
- (17) Wang, S. W.; Wang, L. J.; Zhang, K.; Zhu, Z. Q.; Tao, Z. L.; Chen, J., Organic Li4C8H2O6 Nanosheets for Lithium-Ion Batteries. *Nano Lett.* **2013**, *13*, 4404-4409.
- (18) Song, Z. P.; Qian, Y. M.; Liu, X. Z.; Zhang, T.; Zhu, Y. B.; Yu, H. J.; Otani, M.; Zhou, H. S., A quinone-based oligomeric lithium salt for superior Li-organic batteries. *Energy Environ. Sci.* **2014**, *7*, 4077-4086.
- (19) Song, Z. P.; Qian, Y. M.; Gordin, M. L.; Tang, D. H.; Xu, T.; Otani, M.; Zhan, H.; Zhou, H. S.; Wang, D. H., Polyanthraquinone as a Reliable Organic Electrode for Stable and Fast Lithium Storage. *Angew. Chem. Int. Ed.* **2015**, *54*, 13947-13951.
- (20) Lee, M.; Hong, J.; Kim, H.; Lim, H. D.; Cho, S. B.; Kang, K.; Park, C. B., Organic Nanohybrids for Fast and Sustainable Energy Storage. *Adv. Mater.* **2014**, *26*, 2558-2565.
- (21) Ishii, Y.; Tashiro, K.; Hosoe, K.; Al-zubaidi, A.; Kawasaki, S., Electrochemical lithium-ion storage properties of quinone molecules encapsulated in single-walled carbon nanotubes. *Phys. Chem. Chem. Phys.* **2016**, *18*, 10411-10418.
- (22) Amin, K.; Meng, Q. H.; Ahmad, A.; Cheng, M.; Zhang, M.; Mao, L. J.; Lu, K.; Wei, Z. X., A Carbonyl Compound-Based Flexible Cathode with Superior Rate Performance and Cyclic Stability for Flexible Lithium-Ion Batteries. *Adv. Mater.* **2018**, *30*, 1703868.
- (23) Wang, S.; Wang, Q. Y.; Shao, P. P.; Han, Y. Z.; Gao, X.; Ma, L.; Yuan, S.; Ma, X. J.; Zhou, J. W.; Feng, X.; Wang, B., Exfoliation of Covalent Organic Frameworks into Few-Layer Redox-Active Nanosheets as Cathode Materials for Lithium-Ion Batteries. *J. Am. Chem. Soc.* **2017**, *139*, 4258-4261.
- (24) Jing, Y.; Liang, Y. L.; Gheytani, S.; Yao, Y., Cross-conjugated oligomeric quinones for high performance organic batteries. *Nano Energy* **2017**, *37*, 46-52.
- (25) Jung, M. H.; Ghorpade, R. V., Polyimide Containing Tricarbonyl Moiety as an Active Cathode for Rechargeable Li-Ion Batteries. *J. Electrochem. Soc.* **2018**, *165*, A2476-A2482.